Intermediate mass fragments emission in the reaction 96 MeV ^{19}F on ^{12}C

C. Bhattacharya, D. Bandyopadhyay, S. K. Basu, S. Bhattacharya, K. Krishan, and G. S. N. Murthy
Variable Energy Cyclotron Centre, 1/AF Bidhan Nagar, Calcutta - 700 064, India

A. Chatterjee, S. Kailas, and P. Singh
Nuclear Physics Division, Bhabha Atomic Research Centre, Mumbai - 400 085, India

(Received 12 April 1996)

The energy distributions of the complex fragments ($3 \leqslant Z \leqslant 11$) emitted in the reaction ^{19}F(96 MeV) + ^{12}C have been measured in the angular range $10° \leqslant \theta_{lab} \leqslant 60°$. The lighter fragments ($3 \leqslant Z \leqslant 6$) have been found to be emitted predominantly due to the asymmetric fissionlike decay of the compound nucleus, whereas the heavier fragments ($Z \geqslant 10$) have been identified as evaporation residues. The shapes of the fragment energy distributions, as well as the total elemental yields for the lighter fragments ($3 \leqslant Z \leqslant 6$) have been explained fairly well by the asymmetric binary fission model. The binary fragment yields from the reaction ^{19}F(96 MeV) + ^{12}C have been compared with those obtained in α(60 MeV) + ^{27}Al and ^{7}Li(47 MeV) + ^{24}Mg reactions, all producing the same composite ^{31}P at same excitation energy. No significant entrance channel asymmetry dependence has been observed. [S0556-2813(96)06211-5]

PACS number(s): 25.70.Jj, 25.70.Gh, 25.70.Lm

I. INTRODUCTION

In recent years, extensive efforts have been made to understand the reaction mechanism of fully energy-damped binary fragments emission from moderately hot, medium mass nuclear systems ($A < 100$). The experimentally measured yields of the energy-damped fragments [1–19] are generally interpreted as originating from either a fusion-fission (FF) process [20–23], or a deep inelastic (DI) orbiting mechanism [24]. In the case of fusion-fission process, an equilibrated compound nucleus (CN) is formed, which decays into various exit channels. The probabilities for such decay depend on the available phase spaces and barrier penetration probabilities for the respective channels. The time scales for these processes are typically of the order of the period of revolution of the composite system, which is required for the complete relaxation of the entrance channel energy and angular momentum. Deep inelastic orbiting, on the other hand, has been described in terms of the formation of a long-lived dinuclear molecular complex with a strong memory of the entrance channel. Both orbiting and fusion-fission processes occur on similar time scale. Moreover, for the light nuclear systems in particular, shapes of the orbiting dinuclear complexes are also quite similar to the saddle and scission shapes obtained in course of evolution of the FF process. Therefore, it is not quite straightforward to differentiate the signatures of the two processes, though quite a few attempts have been made in this direction [6,8,10].

It is apparent from the above discussion that the study of the entrance channel asymmetry dependence of the fragment yield may provide us with some important clues regarding the competition between the fusion-fission and orbiting processes. Experimentally, the entrance channel dependence of the fragment yields may be estimated from the study of the decay of a given composite system at a given excitation energy, populated via different entrance channel routes. In recent years, several measurements on the mass asymmetry dependence of the energy-damped fragment yields have been done for lighter composite systems ($A < 50$). The strong entrance channel dependence of the back angle yield of the fragments emitted in the reactions ^{28}Si + ^{12}C and ^{16}O + ^{24}Mg has been indicative of the signatures of orbiting process [2,3,6,10]. On the other hand, the experimental data for the fragment yields from the nearby systems ^{31}P + ^{16}O, ^{35}Cl + ^{12}C, and ^{23}Na + ^{24}Mg [8,13], could be explained fairly well in terms of asymmetric binary fission of the ^{47}V compound nucleus. Recent measurements of binary fragment yields by Anjos *et al.* [16], for the reactions ^{17}O + ^{11}B, ^{18}O + ^{10}B, and ^{19}F + ^{9}Be also have been found to be explained only in terms of the decay of ^{28}Al compound nucleus. Interestingly, back-angle enhancement of elastic and inelastic channels also has been observed in the reactions ^{18}O + ^{10,11}B [11], which may be indicative of the presence of DI orbiting process in the ^{28,29}Al composite system.

It is, thus, evident that some amount of ambiguity still persists in understanding the nature of competition between two mechanisms in the mass region $A \sim 30-50$. This prompted us to investigate the entrance channel asymmetry dependence of intermediate mass fragments (IMF) emission from the light mass nucleus ^{31}P, which is lying in between the two previously studied systems in this mass region, i.e., ^{28}Al and ^{40}Ca. In the present paper, we report the measurement of IMF yields from the composite system ^{31}P having an excitation energy of $\sim$60 MeV, produced in the reaction 96 MeV ^{19}F on ^{12}C. Fragment yields from the same composite system at the same excitation energy, obtained from the reactions 60 MeV α + ^{27}Al [9] and 47 MeV ^{7}Li + ^{24}Mg [17] are compared with the present data to estimate the nature of the entrance channel asymmetry dependence of IMF yields.

The paper has been arranged as follows. The experimental setup is described in Sec. II, in brief. The experimental results are presented in Sec. III. In Sec. IV, theoretical analysis of the data are discussed in detail. Finally, the summary and conclusion are given in Sec. V.

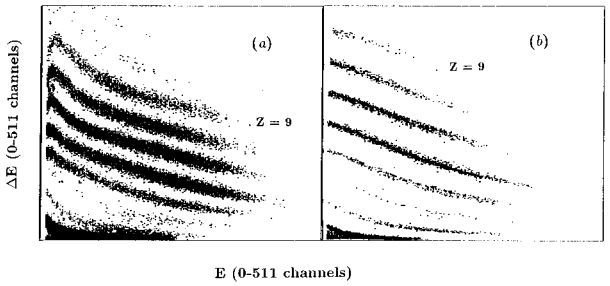

FIG. 1. E vs ΔE plots for (a) gas and (b) SS telescopes at $\theta_{\rm lab}=30°$.

II. EXPERIMENTAL DETAILS

The experiment has been performed at Bhabha Atomic Research Centre – Tata Institute of Fundamental Research 14UD Pelletron Accelerator Laboratory, Mumbai using 96 MeV ^{19}F beam. The target was made by evaporation of natural carbon having a thickness of $\simeq 125$ μg/cm^2. The beam size on the target was typically 1–1.5 mm wide and the typical beam current was 10–90 nA. The emitted fragments were detected in two detector telescopes. One of them was a gas telescope consisting of a gas ΔE and a Si(Li) E (2 mm) detector, and the other one was a full solid state (SS) telescope consisting of 10 μm Si(SB) ΔE and a Si(Li) E (2 mm) detector. The gas ΔE detector was an ionization counter of axial configuration [25], continuous flow type and was filled with P10 gas (90%Ar+10%CH_4) at 90 Torr nominal pressure. Gas pressure was maintained constant to within $\pm$ 2 Torr. A thin polypropylene film of thickness 1.5 μm was used for the window of the gas detector. Typical solid angles were 1.3 msr and 1.5 msr for gas and SS telescopes, respectively. Analog signals from the detectors were processed using standard electronics before being fed to the computer for on-line data acquisition. Carbon build up on the target was monitored at regular intervals during the course of the experiment and was found to be negligible.

The charge resolution obtained in this experiment are illustrated by the ΔE vs E plot displayed in Fig. 1. Well-separated ridges are clearly seen corresponding to elements having atomic numbers up to $Z=11$. The telescopes were calibrated using elastically scattered F ion from Au and C targets. Absolute energy calibrations of the E and ΔE detectors for the two telescopes were done separately using standard kinematics and energy-loss calculations. Typical energy resolutions obtained were 1.5% (E) and 10% (ΔE) for the gas telescope and 2.1% (E) and 3.9% (ΔE) for the SS telescope, respectively. The measured energies have been corrected for the energy losses at the target (for both the telescopes) and at the entrance window (for gas telescope only) by incorporating a single average thickness correction for each fragment energy [9]. Experimental cutoffs thus obtained were typically 4 MeV for lithium, 10 MeV for oxygen, and 14 MeV for sodium.

III. EXPERIMENTAL RESULTS

A. Inclusive energy distributions

Inclusive energy distributions for various fragments ($3\leqslant Z\leqslant 11$) have been measured in the angular range of

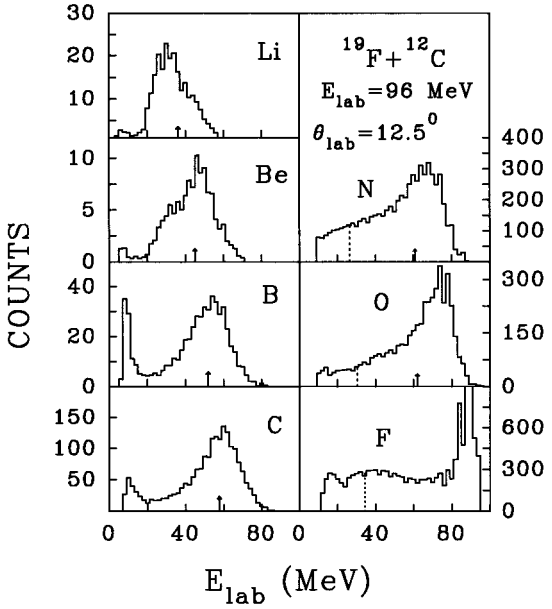

FIG. 2. Inclusive energy spectra of different fragments measured at $\theta_{\rm lab}=12.5°$ (solid histograms). The vertical arrows correspond to the expected fission fragment kinetic energies. The dashed lines correspond to the average energy of the recoiling nuclei.

10°–60°. This covered backward angles in the center of mass (c.m.) frame up to $\sim$140°, because of the inverse kinematics of the reaction. The energy spectra of the emitted fragments ($3\leqslant Z\leqslant 9$) at an angle 12.5° have been shown in Fig. 2. The systematic errors in the data, arising from the uncertainties in the measurements of solid angle, target thickness, and the calibration of current digitizer have been estimated to be $\approx$ 10%. The energy spectra for the lighter fragments ($3\leqslant Z\leqslant 6$) exhibit strong peaking in energy (Fig. 2). The peaks are nearly Gaussian in shape centered close to the expected kinetic energies for the fission fragments obtained from the Viola systematics corrected by the corresponding asymmetry factors [10] (indicated by arrows). The increasing yields at lower energies are due to the second kinematical solution which is a clear signature of the binary nature of the emission process. In the following sections, the properties of these binary fragments will be dicussed in greater detail.

The shapes of the energy spectra for the fragments with $Z=7$–9 are found to differ from those observed for the lighter fragments because in the former cases there may be additional contributions from both deep inelastic (DI) as well as quasi elastic (QE) processes. The quasi elastic bumps occur at the higher energy part of the spectra and their contributions fall off rapidly as one moves away from the grazing angle. On the other hand, the lower energy part of the energy spectra of these fragments arises predominantly from the deep inelastic processes. Moreover, there is a small contribution from the evaporation residues (ER) in the case of flourine ($Z=9$) fragments.

Figure 3 shows the energy distributions of the heavier fragments (Ne, Na), which are essentially evaporation residues. The predictions of the LILITA code [26] calculations (shown by histograms in Fig. 3) are in good agreement with

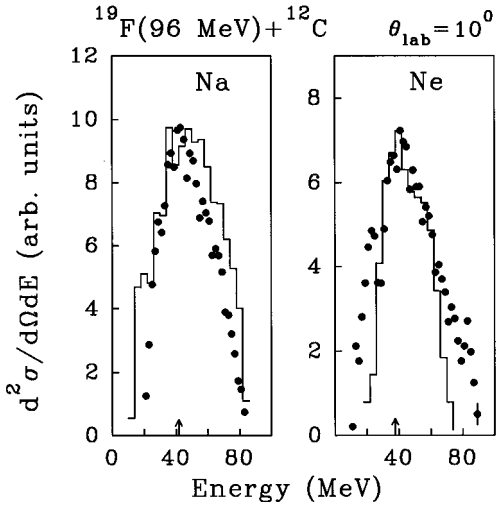

FIG. 3. Inclusive energy spectra for the fragments Ne and Na measured at $\theta_{\rm lab}=10°$ (filled circles). The solid histograms are the results from the code LILITA and the arrows indicate the energy corresponding to $v_{\rm cn}\cos\theta_{\rm lab}$.

the experimental data (solid points). The centroids of the distributions lie close to the energies (shown by the arrows in Fig. 3) corresponding to $v_{\rm cn}\cos\theta_{\rm lab}$, $v_{\rm cn}$ being the compound nuclear velocity. This is in agreement with Morgenstern systematics [27] for fusion reactions with full linear momentum transfer.

B. Angular distributions

The center of mass angular distributions of the fragments ($3\leqslant Z\leqslant 8$) have been displayed as a function of c.m. angle ($\theta_{\rm c.m.}$) in Fig. 4. The transformations from the laboratory to

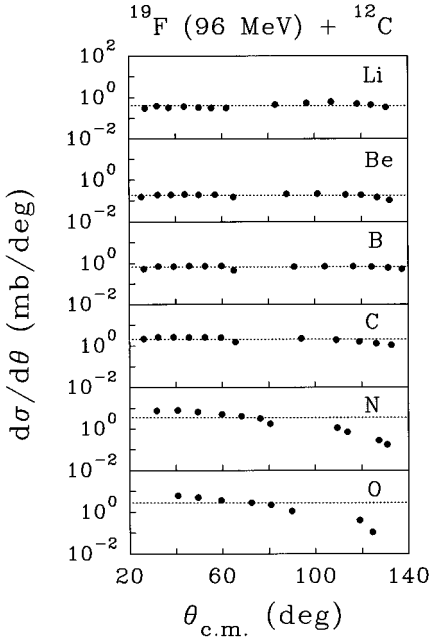

FIG. 4. Center-of-mass angular distributions, $d\sigma/d\theta$ for different fragments (filled circles). The dashed lines correspond to fissionlike angular distribution ($d\sigma/d\Omega\sim a/\sin\theta_{\rm c.m.}$) fits to the data.

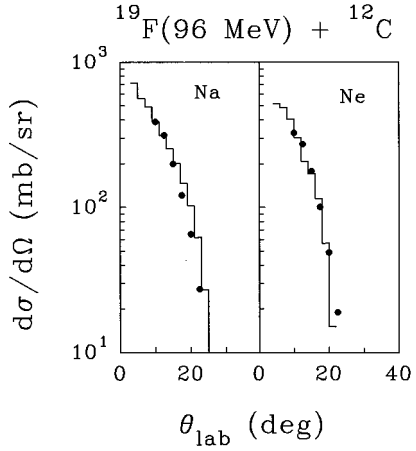

FIG. 5. Angular disributions $d\sigma/d\Omega$, of the fragments Ne and Na, plotted as a function of the laboratory angle (filled circles). The solid histograms are the predictions of the statistical code LILITA.

the c.m. systems have been done with the assumption of a two-body kinematics averaged over total kinetic energy distributions [10]. It is seen from Fig. 4 that, for the lighter fragments ($3\leqslant Z\leqslant 6$), the values of $d\sigma/d\theta_{\rm c.m.}$ are almost constant over the whole range of c.m. angles. Alternatively, $d\sigma/d\Omega$ would have a $\sim 1/\sin\theta_{\rm c.m.}$ type of angular variation, which is characteristic of the fissionlike decay of an equilibrated compound nuclear system. The angular distributions of the fragments with $Z=7$ and 8, are found to be more forward peaked, indicating the presence of contributions from peripheral reactions.

The angular distributions of the heavier fragments ($Z=10,11$) have been displayed in Fig. 5. The data (filled circles) have been compared with the theoretical predictions of the respective ER angular distributions obtained using the statistical Monte Carlo code LILITA (solid histograms). The calculated values have been normalized to match the experimental data at forward angles for $Z=10$. It is seen that the experimental angular distributions are fairly well reproduced by the calculations.

C. Fragment kinetic energies

The average total kinetic energies in the center of mass, $E_K^{\rm tot}$ have been displayed as a function of scattering angle for the fragments ($3\leqslant Z\leqslant 6$) in Fig. 6. The average fragment kinetic energies in the center of mass have been obtained from the respective laboratory values assuming two body kinematics. It is observed from Fig. 6 that $E_K^{\rm tot}$ values are almost constant for each of the exit channel indicating that the lifetime of the dinuclear complex is longer than the time needed to completely damp the energy in the relative motion [28–31]. The predictions of Viola systematics [32] for fission fragment kinetic energies, corrected by an asymmetric factor [10], have been shown by dotted lines in Fig. 6. The $E_K^{\rm tot}$ values predicted from Viola systematics are found to be in good agreement with the experimental data.

D. Fragment average velocities

The average velocities of the fragments have been computed from the measured energies and from the Z values using the empirical relation [33]

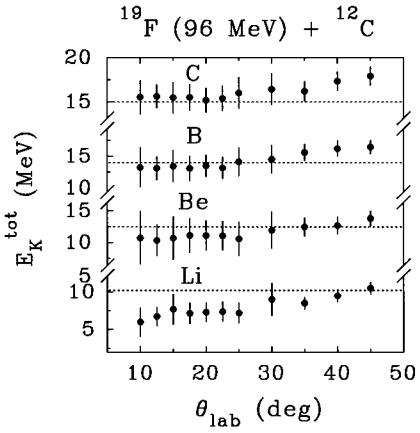

FIG. 6. Average total kinetic energies of the fragments in the center of mass, $E_K^{\rm tot}$ plotted as a function of laboratory angle, $\theta_{\rm lab}$ (filled circles). The predictions of the Viola systematics are shown by dashed lines.

$$A = Z \times (2.08 + 0.0029 \times Z). \tag{1}$$

The average velocities of the fragments ($3 \leqslant Z \leqslant 6$) have been plotted in the ($v_\parallel$) vs ($v_\perp$) plane in Fig. 7. It is seen that the average velocities fall on a circle centered around v_{cn}, which means that the average velocities (as well as kinetic energies) of the fragments are independent of the c.m. emission angles. This clearly indicates that these fragments are emitted from a fully equilibrated CN emission source with full momentum transfer. The magnitude of the average fragment velocities (i.e., the radii of the circles in Fig. 7) increases with the decrease of fragment mass, which is indicative of the binary nature of the emission.

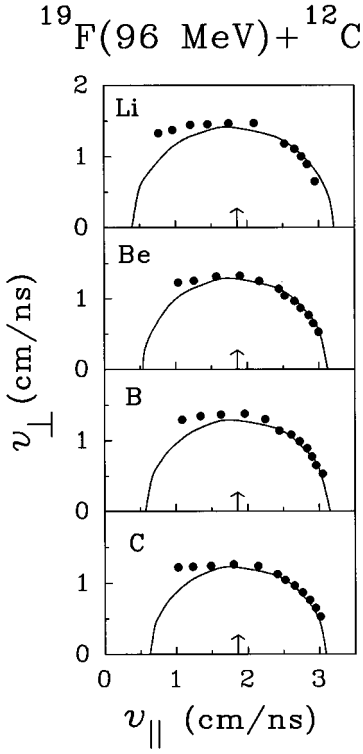

FIG. 7. Average velocities of various fragments plotted as a function of velocities parallel ($v_\parallel$) and perpendicular ($v_\perp$) to the beam direction. The arrow indicates the velocity of the compound nucleus.

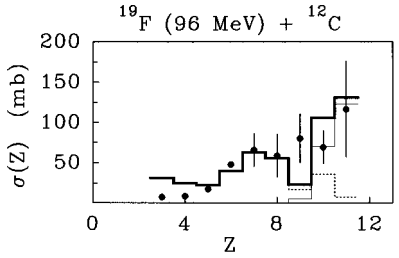

FIG. 8. Total elemental cross sections for different fragments plotted as a function of the fragment charge. The filled circles are the experimental data. The dashed histogram is the contribution of asymmetric fission process (FF) (corrected for secondary deexcitation) and thin solid histogram is the contribution from the evaporation residue (ER). The total (FF+ER) yields are represented by the thick solid histogram.

E. Total elemental cross sections

Total elemental cross sections, $\sigma(Z)$, plotted as a function of atomic number Z of the detected fragments have been displayed in Fig. 8. Filled circles represent the experimental estimates of $\sigma(Z)$, which have been obtained by integrating the energy spectra (Fig. 2) over the whole energy and angular range. The details of the integration procedure are given in Ref. [9]. Total uncertainties in the estimation of $\sigma(Z)$ due to experimental threshold and the limited angular range of the data has been estimated to be typically 5% for Li, 3% for Be, 7% for B, 9% for C, 31% for N, 44% for O, 37% for F, 29% for Ne, and 47% for Na. As the angle increases, the yield falls off faster for heavier fragments. The relatively large uncertainties in N, O, F, Ne, and Na are due to the absence of the data at more forward angles below 10°. The cross sections are found to vary between 8 mb for $Z=3$ and 115 mb for $Z=11$.

IV. ANALYSIS AND DISCUSSIONS

A. Asymmetric Binary Fission of the CN

Several attempts have been made in recent years to explain the phenomena of IMF emission in the framework of generalized fusion-fission models [20–22], where the classical transition state picture of fission [34] have been extended to estimate the asymmetric fission yields of the nuclei lying below the Businaro-Gallone point [35]. In these models, fragment emission takes place as a result of the gradual shape evolution of the compound nucleus from spherical to highly deformed ones resembling a binary system connected by a neck. Subsequently, it may reach the conditional saddle point [20] corresponding to any possible exit channel configuration and then it scissions into two fragments. The yields of the fragments depend on the barrier heights at the conditional saddle points corresponding to the respective exit channel configuration.

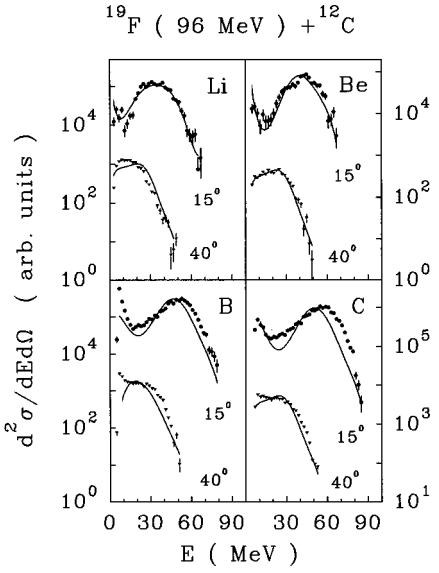

FIG. 9. $d^2\sigma/dEd\Omega$ for different fragments plotted as a function of the laboratory kinetic energy of the fragments. The filled circle and inverted triangle correspond to the experimental data for the laboratory angles ($\times$ multiplication factor) of 15°($\times 1$) and 40°($\times 10^{-2}$), respectively. The solid curves are the results of the asymmetric binary fission calculations.

1. Fragment energy spectra

The center of mass kinetic energy distribution of the binary fragments, according to a simplified version of Ref. [20], may be written as [36]

$$P(x)dx \sim \exp\left(-\frac{x}{T}\right)dx, \tag{2}$$

where $x = E^{\rm kin}_{\rm c.m.} - E_B$, and E_B is the Coulomb barrier in the exit channel and T is the temperature of the compound nucleus.

Assuming an isotropic c.m. angular distribution, the energy spectrum [Eq. (2)] of the fragments can be transformed to the laboratory system [36]. The exit channel Coulomb barrier E_B has been calculated using the prescription of Ref. [17]. In Fig. 9, experimental energy distributions for the fragments ($3 \leqslant Z \leqslant 6$) at 15° (filled circles) and 40° (inverted triangles) have been displayed along with the predictions of the same obtained from asymmetric binary fission model (solid curves). It is observed from Fig. 9 that the theoretical predictions reproduce fairly well the shapes of the energy distributions for the fragments $3 \leqslant Z \leqslant 6$ at both the angles. This is indicative of the fact that the IMF emission is predominantly of compound nuclear origin and can be fairly well explained in terms of asymmetric binary splitting of a deformed compound system.

2. Fragment average kinetic energy

Asymmetric binary fission, which accounts for the emission of IMF's from the systems lying below the Businaro-Gallone point [35], is a dynamical process consisting of gradual change of shape, formation of neck and finally separation into two fragments at the scission point. Therefore, the fission dynamics should be properly taken care of while evaluating relevant physical observables. In the present work, the mean kinetic energies of different fragments have been calculated using a dynamical model of IMF emission [37]. Here, in absence of any precise knowledge about the mechanism of energy sharing between the intrinsic excitation and collective degrees of freedom, it is assumed that a random fraction of the initial excitation energy of the compound nucleus goes to collective degree of freedom to generate dynamics. The fission probability $P(f,\alpha|l)$ for any configuration α at angular momentum l is then calculated from a Monte Carlo simulation of a large number of dynamical trajectories. Then, the average total kinetic energy $\langle E_K^{\rm tot}\rangle$ of the fragments in the center of mass for the exit channel configuration α is calculated using the following expression [37]:

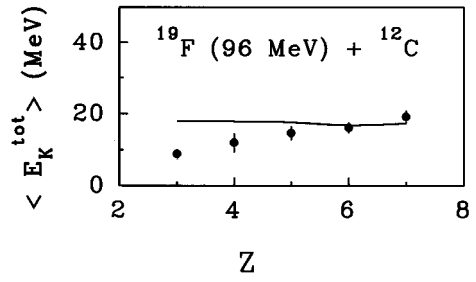

FIG. 10. Angle averaged total c.m. kinetic energies of the fragments plotted as a function of the fragment charge. The filled circles correspond to the experimental data and the solid curve is the theoretical calculation of the same (see text).

$$\langle E_K^{\rm tot}\rangle = \frac{\sum_{l=0}^{l_{\rm cr}}(2l+1)E_K^{\rm tot}(\alpha)P(f,\alpha|l)}{\sum_{l=0}^{l_{\rm cr}}(2l+1)P(f,\alpha|l)}, \tag{3}$$

where $l_{\rm cr}$ is the critical angular momentum for fusion. The present experimental estimate of total fusion cross section has not been used to calculate the value of $l_{\rm cr}$, as there are relatively large uncertainties in the measured cross sections of the heavier elements, which are essentially evaporation residues. Instead, the value of $l_{\rm cr}$ ($= 21\hbar$) has been taken from the tabulation of heavy ion reaction parameters by Wilcke *et al.* [38], which has been obtained from the systematic study of the fusion cross section data for ^{19}F + ^{12}C system at somewhat lower energies [39]. Same value of $l_{\rm cr}$ also has been obtained by heavy ion trajectory calculation [40]. The theoretical predictions of the mean total kinetic energies for the fragments with $3 \leqslant Z \leqslant 7$, calculated using Eq. (3), have been displayed in Fig. 10 (solid curve) along with the experimental estimates of the same (filled circles). It is clearly evident from Fig. 10 that the theoretical predictions of $\langle E_K^{\rm tot}\rangle$ are in fair agreement with the corresponding experimental results except for lighter fragments ($Z = 3,4$), where the theory slightly overpredicts the data.

3. Total fragment yields

The IMF emission cross section for various fragments can be calculated using binary fragmentation model from simple phase-space consideration. Assuming that the reactants fuse completely to form an excited compound nucleus which sub-

sequently decays statistically into various channels, the total emission cross section for a fragment of charge Z can be calculated using the expression [22]

$$\sigma(Z)=\pi\lambda\!\!\!^{-2}\sum_{l=0}^{l_{\rm cr}}(2l+1)\frac{\Gamma_Z(l)}{\Gamma_{\rm tot}}, \tag{4}$$

where $\lambda\!\!\!^{-}$ is the de Broglie wavelength, $\Gamma_Z(l)$ is the decay width for the fragment of charge Z, and $\Gamma_{\rm tot}$ is the total decay width. The ratio $\Gamma_Z(l)/\Gamma_{\rm tot}$ represents the probability of decay of the compound nucleus of angular momentum l in a particular channel with charge Z. The decay width $\Gamma_Z(l)$, calculated in the transition state formalism [4], is given by

$$\Gamma_Z(l)\propto T_Z(l)\left[\frac{E}{E-B_Z(l)}\right]^2\exp(2\{a[E-B_Z(l)]\}^{1/2} -2(aE)^{1/2}), \tag{5}$$

where E is the compound nucleus excitation energy and $B_Z(l)$ is the barrier height at the conditional saddle point. The conditional saddle points have been derived by extremizing the potential energy of the deformed nuclear system [22]. The temperature $T_Z(l)$ is calculated from the relation $E-B_Z(l)=aT_Z^2(l)$, a $(=A_{\rm CN}/8)$ is the level density parameter.

The charge distribution for the primary fragments may further be modified due to (*a*) contributions from secondary fission, and, (*b*) deexcitation of the excited primary fragments by evaporation of light particles. A detailed analysis of the secondary deexcitation process in the decay of light compound systems may be found in Ref. [21]. Secondary fission, which is characterized by the emission of light particles prior to fission, is unlikely in light systems [21], and therefore, was not considered in the present calculation. Secondary decay of the excited primary fragments were simulated using the evaporation code LILITA. The primary mass distributions were taken from transition-state model. The intrinsic excitation energy of the compound system was divided in the ratio of the fragment masses. The spins transferred to the fragments were computed in the sticking limit of the two fragments at the scission configuration [22]. In the present case, calculation indicates that the secondary light particle emission does not affect the primary charge distributions of the lighter fragments (Z = 3–6) in a significant manner, with the exception of Be. In the case of Be, each primary fragment of ^{8}Be, being unstable, should decay into a pair of α particles. As it is difficult to estimate the yield of ^{8}Be experimentally, the contribution from ^{8}Be is not taken into account while calculating the total yield of Be theoretically. In the case of fragments with charge $Z\geqslant 7$, however, the primary fragment yields are found to be significantly modified due to additional contributions from the secondary deexcitation of heavier counterparts of various asymmmetric decay channels. The final yield of the fragments, $\sigma_{\rm fin}$, has been calculated using the following relation [40]:

$$\sigma_{\rm fin}(Z)=\sigma_{\rm pri}(Z)-\sum_{\Delta Z}\sigma_{\rm pri}(Z)P_Z(\Delta Z) +\sum_{\Delta Z}\sigma_{\rm pri}(Z+\Delta Z)P_{Z+\Delta Z}(\Delta Z), \tag{6}$$

where $\sigma_{\rm pri}(Z)$ is the yield of the primary fragment with charge Z (Eq. 4) and $P_Z(\Delta Z)$ is the decay probability for the primary fragment of charge Z in the decay mode where it loses ΔZ amount of charge through evaporation, leading to the final fragment of charge $Z-\Delta Z$. The decay probabilities have been computed for ΔZ = 1 and 2. The ratio $\sigma_{\rm fin}(Z)/\sigma_{\rm pri}(Z)$ for Z = 7, 8, 9, 10, and 11 then have been estimated using Eq. 6 to be 2.06, 1.82, 0.43, 1.56, and 0.32, respectively. It is thus clear that secondary deexcitation modifies significantly the yields of the heavier fragments.

The predicted FF yields (properly corrected for secondary deexcitation) for the fragments with $3\leqslant Z\leqslant 11$ have been displayed in Fig. 8 (short dashed histogram). The estimated total experimental yields have been represented by filled circles. The thin line histogram in Fig. 8 displayed the contribution of the ER to the total elemental yields calculated using statistical evaporation code LILITA. The calculated total (FF + ER) yields have been represented by thick solid histograms. It is seen that the total emission cross sections predicted by the asymmetric fission model are in fair agreement with the corresponding experimental values for the lighter fragments ($Z=3$–8). For Z = 9 fragment, there may be additional contributions from other direct reaction processes. Such processes also may have some contributions to the yields of Z = 7 and 8 fragments (as already indicated in Sec. III). On the other hand, statistical evaporation process plays a dominant role in the production of heavier fragments ($Z=10$, 11). The experimental yields for these fragments are fairly well explained by the sum total of the predicted yields of the two (FF + ER) processes (thick solid histogram), where the ER contributions have been computed with the help of the statistical evaporation code LILITA.

B. Fusion-fission and orbiting processes in $A=31$ system

It is now well established that in both FF and orbiting processes, only a few partial waves near the grazing angular momentum are involved. Therefore, the number of open channels (NOC) available to carry away the grazing angular momentum L_g of the compound nucleus is likely to play an important role in determining the mechanism of its decay. It has been shown that for many light heavy-ion systems there is a strong correlation between the existence of very low NOC and the occurrence of resonant behavior and back angle enhancement in the elastic, inelastic, or α transfer channels [41]. Since deep inelastic orbiting in heavier systems and molecular resonance in lighter systems are likely to have a similar origin, attempts also have been made to understand the systematics of DI orbiting mechanism by suitable generalizations of the original NOC model [42]. Assuming binary reaction channels only, the number of open channels, $N^J(E_{\rm c.m.})$, is calculated as a triple summation over all possible binary reaction channels, all possible angular momentum couplings and all possible energy distributions between the fragments. Then the number of open channels

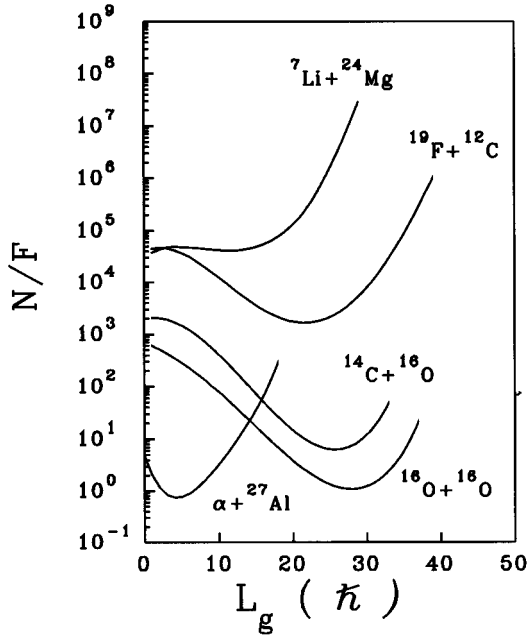

FIG. 11. Number of open channels for the decay of the compound nucleus normalized to the incident flux, N/F, plotted as a function of the grazing angular momentum L_g.

per unit of incident flux, N/F, which will be referred to as NOC in the text, is defined as [42]

$$N/F = N^J(E_{\text{c.m.}})/F^J(E_{\text{c.m.}}), \tag{7}$$

where

$$N^J(E_{\text{c.m.}}) = \sum_{A_1+A_2=A_{CN}} \sum_{J=I_1+I_2+l} \sum_{E_{\text{ex}}=E_1+E_2+Q_{12}+E_r} T_l(E_r), \tag{8}$$

and the incident flux $F^J(E_{\text{c.m.}})$ is given by

$$F^J(E_{\text{c.m.}}) = \frac{\pi}{k^2} g_J \sum_{J=j_1+j_2+L} T_L(E_{\text{c.m.}}). \tag{9}$$

Here $g_J=(2J+1)/[(2j_1+1)(2j_2+1)]$, j_1 and j_2 being the intrinsic spins of the reactants and L is the angular momentum of their relative motion. I_k, E_k $(k=1,2)$ are the intrinsic spins and excitation energies of the fragments, l, E_r are the orbital angular momentum and energy of their relative motion, Q_{12} is the ground state Q value of decay and $T_l(E_r)$, $T_L(E_{\text{c.m.}})$ are the transmission coefficients of the outgoing and incoming channels, respectively. The transmission coefficients have been calculated semiclassically using the inverted parabolic barrier approximation [43] and the barrier heights have been calculated by incorporating macroscopic proximity potential [44] in the Wilcke parametrization of barrier heights [38]. In the case of spin zero particles, N/F is calculated with $J=L_g$ and in other cases largest possible values of J are considered.

In Fig. 11, the NOC's calculated using Eq. 7 for the $A=31$ systems, i.e., ^{19}F + ^{12}C, ^{7}Li + ^{24}Mg, and α + ^{27}Al have been plotted as a function of grazing angular momentum L_g. The values of L_g, which are related to the the respective bombarding energies, are 20, 20, and 24 for the reactions α(60 MeV)+Al, Li(47 MeV)+Mg, and F(96 MeV)+C, respectively. For the sake of comparison, NOC's for the two neighboring systems $A=30,32$ (^{14}C + ^{16}O and ^{16}O + ^{16}O) also have been calculated and plotted in the same figure. It is seen from Fig. 11 that the NOCs for ^{19}F + ^{12}C, ^{7}Li + ^{24}Mg systems at their minima (which nearly correspond to the present bombarding energies) are much higher than those for ^{14}C + ^{16}O and ^{16}O + ^{16}O systems. Incidentally, both ^{14}C + ^{16}O and ^{16}O + ^{16}O systems have been found to show strong resonant behavior [42]. Therefore, the large NOC's available for the decay of ^{19}F + ^{12}C and ^{7}Li + ^{24}Mg systems (e.g., $\sim 10^4$ times larger than ^{16}O + ^{16}O case) are indicative of the dominance of FF origin of the binary energy-damped yields in these cases. In the case of α + ^{27}Al system, however, L_g for the present reaction is larger than the value at which NOC is minimum. Therefore, any orbiting behavior of the energy damped fragment yield is unlikely to show up in the present reaction. Incidentally, experiments even at lower bombarding energies corresponding to the minima of the NOC curve have shown that, though the NOC value was small in this case, there was no indication of orbiting [45].

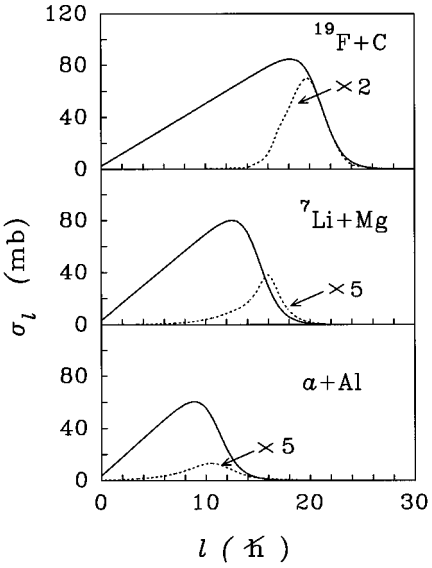

FIG. 12. Partial-wave distributions of fusion (solid curve) and FF (dashed curves) cross sections for the reactions ^{19}F(96 MeV) + ^{12}C, ^{7}Li(47 MeV) + ^{24}Mg and α(60 MeV) + ^{27}Al.

The conjecture of fusion-fission origin of the IMF emission from $A=31$ systems has been further elucidated from the study of entrance channel dependence of the total IMF yields. Since the average spins of the compound nuclei under consideration are different, it would be worthwhile to study the variation of FF contribution with the spin of the compound systems before one arrives at any conclusion regarding possible origin of the energy damped fragment yields. The calculated fusion partial wave distributions for the three systems under consideration, i.e., ^{19}F + ^{12}C at 96 MeV, ^{7}Li + ^{24}Mg at 47 MeV [17], and α + ^{27}Al at 60 MeV [9], all populating the same compound nucleus at same excitation energy, are displayed in Fig. 12. The calculations have been

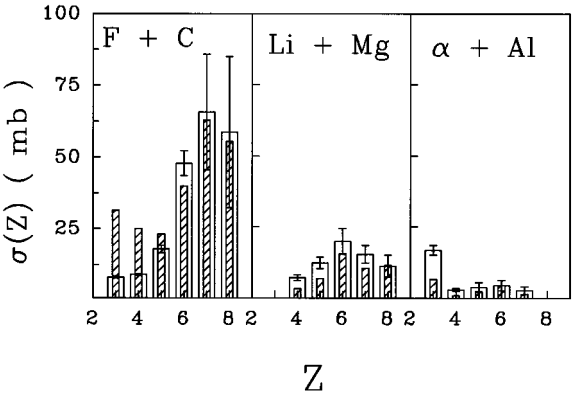

FIG. 13. Experimental charge distributions of the fissionlike yields produced in the reactions ^{19}F(96 MeV) + ^{12}C, ^{7}Li(47 MeV) + ^{24}Mg [17] and α(60 MeV) + ^{27}Al [9]. The experimental data are represented by the open histograms and the theoretical predictions are represented by hatched histograms.

done in the framework of asymmetric binary fission model [22], with the value of the diffuseness parameter taken to be $1\hbar$. It is evident from Fig. 12 that the contributions from FF increases for more symmetric target projectile combination. Moreover, FF is confined to the highest reaction partial waves. Figure 13 shows the plot of total elemental cross sections as a function of Z for the three reactions mentioned above. The open histograms represent the experimental data whereas the predictions of binary fission model are represented by hatched histograms. It is seen from Fig. 13 that, despite different partial wave distributions (Fig. 12), the three experimental charge distributions are similar in shape. The fragment yields increase from α + ^{27}Al (l_{cr} = 12) to ^{7}Li + ^{24}Mg (l_{cr} = 16) and to ^{19}F + ^{12}C (l_{cr} = 21), due to the variation of l_{cr} as well as due to the increased yield of FF for more symmetric entrance channels as shown in Fig. 12. For the fragments with $Z=3$ in α+Al system and $Z=7,8$ in F+C system, the predicted yields underestimate the observed experimental yields. This is due to the fact that peripheral reactions also would contribute substantially to the yields of these fragments. Thus the present set of data does not demonstrate any significant entrance channel effects as observed in the cases of orbiting reactions [2,3,6,10]. Moreover, the fragment yields also are found to be in fair agreement with the the transition-model predictions. In Fig. 14, the ratio of yields of the fragments B and C, σ_B/σ_C, has been plotted for the three systems mentioned above as a function of the entrance channel asymmetry, $|(A_P-A_T)/(A_P+A_T)|$, (A_P, A_T are the projectile, target masses, respectively). It is seen that the ratio is weakly dependent on the entrance channel asymmetry, which is in contrast with the large entrance channel dependence of the same observed in the case of orbiting reactions [13]. Moreover, the experimental estimates of the above ratios also are found to be in fair agreement with the respective theoretical predictions of the same. This is further indicative of the fusion-fission origin of the strongly damped fragment yields from $A=31$ systems.

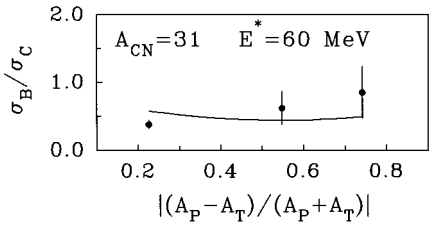

FIG. 14. Ratio of B and C yields, σ_B/σ_C, plotted as function of entrance channel asymmetry, $|(A_P-A_T)/(A_P+A_T)|$ for $A=31$ compound nucleus.

V. SUMMARY AND CONCLUSION

The inclusive double differential cross sections for fragments ranging from Li to Na emitted in the reaction ^{19}F(96 MeV) + ^{12}C have been measured. Total emission cross sections for various fragments have been estimated from the double differential cross-section data. The c.m. angular distributions for the lighter fragments $3\leqslant Z\leqslant 6$ are found to have a $\sim 1/\sin\theta_{\text{c.m.}}$ dependence signifying that these fragments are emitted from a long-lived composite. However, the angular distribution for the fragments N and O are more forward peaked indicating additional contributions from other reaction processes in these cases. From the rapidity analyses, it has been found that the lighter fragments $3\leqslant Z\leqslant 6$ are emitted from fully equilibrated source moving with compound nuclear velocity. The shapes of the energy distributions computed from the asymmetric binary fission model are found to be in good agreement with the experimental data for the fragments $3\leqslant Z\leqslant 6$. The average kinetic energies of the fragments calculated in the framework of dynamical theory of asymmetric fission are also in fair agreement with the experimental estimates of the same except for Li and Be, where the theoretical predictions slightly overpredict the data. In the case of total fragment yields, the data for the fragments ($Z=3$–8) are fairly well explained in the fusion-fission picture, when the contributions of secondary deexcitation of heavy fragments are taken into account. The corrections to the primary fragment yield due to secondary deexcitation are found to be more significant for heavier fragments ($Z>6$ in particular). Besides, there may be additional contributions to the fragment yield from peripheral reactions in the case of O and N. The heavier fragments Ne and Na are found to be essentially evaporation residues and their angular and energy distributions are satisfactorily explained by the standard statistical model calculations.

The competition between fusion-fission and DI orbiting have been investigated by calculating the NOC for different entrance channel combinations, i.e., ^{19}F + ^{12}C, ^{7}Li + ^{24}Mg, and α + ^{27}Al, leading to $A=31$ composite. The present bombarding energies nearly correspond to the minima of the respective NOC curves for the first two systems, whereas for α + ^{27}Al system the corresponding L_g is larger than the value where the minima occurs. The NOC values in the first two cases are found to be quite large, thus favoring fusion-fission than DI orbiting in these cases. For the α + ^{27}Al system, the incident energy (or L_g) of the

reaction considered here is away from the correspoding NOC minima and the results are fairly well explained in the framework of transition-state model. Inspite of the different fission partial wave distributions, comparison of integrated yield distributions in all three cases does not reveal any prominent entrance channel dependence. The ratio of integrated yields of B and C, has been found to be weakly dependent on the entrance channel asymmetry. Thus, it may be inferred that fusion-fission, rather than DI orbiting, is the dominant mechanism of strongly energy damped fragment emission from ^{31}P composite system.

ACKNOWLEDGMENTS

The authors thank the Pelletron accelerator staff for the smooth running of the machine and Mr. D.C. Ephraim for making the targets. The authors would like to thank Dr. A. Roy and Dr. M. Ismail for making available the code LILITA.

[1] D. Shapira, R. Novotny, Y.D. Chan, K.A. Erb, J.L.C. Ford, Jr., J.C. Peng, and J.D. Moses, Phys. Lett. **114B,** 111 (1982).

[2] D. Shapira, D. Schull, J.L.C. Ford, Jr., B. Shivakumar, R.L. Parks, R.A. Cecil, and S.T. Thornton, Phys. Rev. Lett. **53,** 1634 (1984).

[3] A. Ray, S. Gil, M. Khandaker, D.D. Leach, D.K. Lock, and R. Vandenbosch, Phys. Rev C **31,** 1573 (1985).

[4] S.J. Sanders, R.R. Betts, I. Ahmad, K.T. Lesko, S. Saini, B. Wilkins, F. Videbaek, and B.K. Dichter, Phys. Rev. C **34,** 1746 (1986).

[5] S.J. Sanders, D.G. Kovar, B.B. Back, C. Beck, B.K. Dichter, D. Henderson, R.V.F Janssens, J.G. Keller, S. Kaufman, T.F. Wang, B. Wilkins, and F. Videbaek, Phys. Rev. Lett. **59,** 2856 (1987); **61,** 2154 (1988); Phys. Rev. C **40,** 2091 (1989); **41,** R1901(1990).

[6] C. Beck, B. Djerroud, B. Heusch, R. Dayras, R.M. Freeman, F. Haas, A. Hachem, J.P. Wieleczko, and M. Youlal, Z. Phys. A **334,** 521 (1989).

[7] M.M. Coimbra, R.M. Anjos, N. Added, N. Carlin, L. Fante, Jr., M.C.S. Figueira, G. Ramirez, E.M. Szanto, and A. Szanto de Toledo, Nucl. Phys. **A535**, 161 (1991).

[8] A. Ray, D. Shapira, J. Gomez del Campo, H.J. Kim, C. Beck, B. Djerroud, D. Blumenthal, and B. Shivakumar, Phys. Rev. C **44**, 514 (1991).

[9] C. Bhattacharya, S.K. Basu, S. Bhattacharya, A. Chakraborty, S. Chattopadhyay, M.R. Dutta Majumdar, K. Krishan, G.S.N Murthy, B. Sinha, M.D. Trivedi, Y.P. Viyogi, S.K. Dutta, and R.K. Bhowmik, Phys. Rev. C **44,** 1049 (1991).

[10] C. Beck, B. Djerroud, F. Haas, R.M. Freeman, A. Hachem, B. Heusch, A. Morsad, M. Youlal, Y. Abe, A. Dayras, J.P. Wieleczko, B.T. Matsuse, and S.M. Lee, Z. Phys. A **343,** 309 (1992).

[11] A. Lepine-Szily, J.M. Oliveira, Jr., P. Fachini, R. Lichenthaler Filho, M.M. Obuti, W. Sciani, M.K. Steinmayer, and A.C.C. Villari, Nucl. Phys. **A539,** 487 (1992).

[12] K. Yuasa-Nakagawa, Y.H. Pu, S.C. Jeong, T. Mizota, Y. Futami, S.M. Lee, T. Nakagawa, B. Heusch, K. Ieki, and T. Matsuse, Phys. Lett. B **283,** 185 (1992).

[13] C. Beck, B. Djerroud, F. Haas, R.M. Freeman, A. Hachem, B. Heusch, A. Morsad, M. Vuillet-A-Cilles, and S.J. Sanders, Phys. Rev. C **47,** 2093 (1993).

[14] R.M. Anjos, N. Added, N. Carlin, L. Fante, Jr., M.C.S. Figueira, R. Matheus, E.M. Szanto, C. Tenrein, A. Szanto de Toledo, and S.J. Sanders, Phys. Rev. C **48,** R2154 (1993).

[15] L. Fante, Jr., N. Added, R.M. Anjos, N. Carlin, M.M. Coimbra, M.C.S. Figueira, R. Matheus, E.M. Szanto, and A. Szanto de Toledo, Nucl. Phys. **A552,** 82 (1993).

[16] R.M. Anjos, N. Added, N. Carlin, L. Fante, Jr., M.C.S. Figueira, R. Matheus, E.M. Szanto, C. Tenrein, A. Szanto de Toledo, and S.J. Sanders, Phys. Rev. C **49,** 2018 (1994).

[17] C. Bhattacharya, D. Bandyopadhyay, G.S.N. Murthy, Y.P. Viyogi, S.K. Basu, K. Krishan, S. Bhattacharya, S. Kailas, A. Chatterjee, and P. Singh, Phys. Rev. C **52,** 798 (1995).

[18] K. Yuasa-Nakagawa, J. Kasagi, T. Nakagawa, S.M. Lee, K. Furutaka, K. Matsuda, and W.Q. Shen, Phys. Rev. C **53,** 997 (1996).

[19] Y.H. Pu, S.M. Lee, S.C. Jeong, H. Fujiwara, T. Mizota, Y. Futami, T. Nakagawa, H. Ikezoe, and Y. Nagame, Z. Phys. A **353,** 387 (1996).

[20] L.G. Moretto, Nucl. Phys. **A247,** 211 (1975).

[21] S.J. Sanders, Phys. Rev. C **44,** 2676 (1991).

[22] C. Bhattacharya and S. Bhattacharya, Phys. Rev. C **43,** 1491 (1991).

[23] T. Matsuse, S.M. Lee, and C. Beck, in *Proceedings of the International Symposium Towards a Unified Picture of Nuclear Dynamics*, Nikko, 1991, edited by Y. Abe, S.M. Lee, and F. Sakata, AIP Conf. Proc. No. 250 (AIP, New York, 1992), p. 112.

[24] B. Shivakumar, S. Ayik, B.A. Harmon, and D. Shapira, Phys. Rev. C **35,** 1730 (1987).

[25] S.K. Bandyopadyay, S.K. Basu, S. Bhattacharya, R.K. Bhowmik, A. Chakrabarty, S.K. Datta, G.S.N. Murthy, and Y.P. Viyogi, Nucl. Instrum. Methods Phys. Res. A **278,** 467 (1989).

[26] J. Gomez del Campo, J.A. Biggerstaff, R.A. Dayars, D. Shapira, A.H. Shell, P.H. Stelson, and R.G. Stokstad, Phys. Rev. C **29,** 1722 (1984).

[27] H. Morgenstern, W. Bohne, W. Galster, K. Grabisch, and A. Kyanowski, Phys. Rev. Lett. **52,** 1104 (1984).

[28] R. Eggers, M.N. Namboodri, P. Gonthier, K. Geoffroy, and J.B. Natowitz, Phys. Rev. Lett **37,** 324 (1976).

[29] P. Braun-Munzinger, T.M. Cormier, and C.K. Gelbke, Phys. Rev. Lett. **37,** 1582 (1976).

[30] T.M. Cormier, P. Braun-Munzinger, P.M. Cormier, J.W. Harris, and L.L. Lee, Jr., Phys. Rev. C **16,** 215 (1977).

[31] J.B. Natowitz, M.N. Namboodri, R. Eggers, P. Gonthier, K. Geoffroy, R. Hanus, C. Towsley, and K. Das, Nucl. Phys. **A277**, 477 (1977).

[32] V.E. Viola, K. Kwiatkowski, and M. Walker, Phys. Rev. C **31,** 1550 (1985).

[33] R.J. Charity, D.R. Bowman, Z.H. Liu, R.J. McDonald, M.A. McMahan, G.J. Wozniak, L.G. Moretto, S. Bradley, W.L. Kehoe, and A.C. Mignerey, Nucl. Phys. **A476,** 516 (1988).

[34] N. Bohr and J.A. Wheeler, Phys. Rev. **56,** 426 (1939).

[35] U.L. Businaro and S. Gallone, Nuovo Cimento **1,** 629 1277 (1955).
[36] T. Kozik, J. Buschmann, K. Grotowski, H.G. Gils, N. Heide, J. Kiener, H. Klewe-Nebenius, H. Rebel, S. Zagromski, A.J. Cole, and S. Micek, Z. Phys. A **326,** 421 (1987).
[37] A. Dhara, C. Bhattacharya, S. Bhattacharya, and K. Krishan, Phys. Rev. C **48,** 1910 (1993).
[38] W.W. Wilcke, J.R. Birkelund, H.J. Wollersheim, A.D. Hoover, J.R. Huizenga, W.U. Schroeder, and L.E. Tubbs, At. Data Nucl. Data Tables **25,** 389 (1980).
[39] R. Bass, *Nuclear Reactions with Heavy Ions* (Springer-Verlag, Berlin, 1980), p. 256.
[40] C. Bhattacharya, S. Bhattacharya, and K. Krishan, Phys. Rev. C **49,** 3147 (1994).
[41] F. Haas and Y. Abe, Phys. Rev. Lett. **46,** 1667 (1981).
[42] C. Beck, Y. Abe, N. Aissaoui, B. Djerroud, and F. Haas, Phys. Rev. C **49,** 2618 (1994).
[43] W. Ford, D.L. Hill, M. Wakano, and J.A. Wheeler, Ann. Phys. (N.Y.) **7,** 239 (1959).
[44] J. Blocki, J. Randrup, W.J. Swiatecki, and C.F. Tsang, Ann. Phys. (N.Y.) **105,** 427 (1977).
[45] A. Ray, S.R. Banerjee, P. Das, A. Mitra, S.K. Basu, and P. Bhattacharya, Phys. Rev. C **51,** R1604 (1995).